# On-line Synergy Identification for Personalized Active Arm Prosthesis: a Feasibility Study

Ricardo Garcia-Rosas, Ying Tan, Denny Oetomo, Chris Manzie

*Abstract*— **The number of degrees of freedom in prosthetic devices today is greater than the number of available electromyographic signals from the residual limb. This potentially causes complex and unintuitive interfaces, which in turn have been cited as a leading cause of prosthetic device abandonment. Synergistic arm prosthesis control allows for an intuitive way to provide additional information to command the motion of the prosthesis by coordinating the motion relationship between the prosthesis and the residual limb. There is a challenge in identifying effective synergies, especially as the motion of an amputee generally differs from the synergy of the typical able-bodied subjects, from person to person, and along the time of prosthesis usage. In this paper, a framework for on-line data driven optimization is proposed to identify the optimal synergy setting for an individual performing a specific task, formulated as an optimization problem based on human motor control. This is done through the characterization of the task by a cost function and the parametrization of the synergy. The proposed framework is able to characterize and identify the synergy of the task of reaching for a given location, with a healthy subject in the loop. The framework is used to drive the motion of an elbow prosthesis using its synergy with the residual shoulder movement of the human subject as input. A simple parametrization for the synergy is used in this paper to demonstrate the idea of the proposed framework. Human-in-the-loop simulation results are presented, showing the feasibility of data driven optimization for on-line synergy identification in the context of an arm prosthesis.**

## I. Introduction

Active arm prostheses are typically commanded with signals from the user's residual limb. However, the degrees of freedom (DOF) in the prosthetic device are typically greater than the number of available electromyographic (EMG) signals from the residual limb, making these interfaces unintuitive. Even if the number of signals is enough, such as with Targeted Muscle Reinnervated (TMR) [1] users, where a large number of EMG signals can be read from the residual limb, coordinating the signals to regulate the motion of a prosthesis is a complex process. These challenges reduce the effectiveness of prostheses and lead to a high degree of device abandonment [2]. It can be argued therefore that EMG can be supplemented by other interfaces, potentially those more intuitive to the intended motion.

The hypothesis of muscle synergies suggests that the central nervous system (CNS) groups muscles together in order to simplify the control of complex coordinated motion [3]. Studies have shown the existence of kinematic synergies that coordinate the motion of DOF in a limb, beyond coordination at muscle level [4]. These differ from postural synergies in their dependence on general motion rather than position. A relationship between muscle and kinematic synergies exists [4], making it possible to use kinematic synergies to represent the synergistic control utilized by the CNS. Kinematic synergies have been the main focus of study in synergistic arm prosthesis control, e.g. to determine motion of an elbow prosthesis through the motion of the residual limb [5]. Synergistic arm prosthesis control allows for an intuitive way to provide additional information to command the motion of prostheses by coordinating the motion relationship between the prosthesis and the residual limb [5].

The majority of current synergistic approaches use artificial neural networks (ANNs) to represent shoulder-elbow synergies [5]–[7]. These ANNs are trained with able-bodied subjects that repeat a set of tasks in order to identify the synergies through supervised learning. The generated ANNs are used to determine elbow prosthesis motion from measured shoulder motion. In some cases, shoulder motion sensors have been complimented with EMG signals, combining kinematic and muscle synergies [8]. Thus providing more data for ANN training and classification, improving their performance. However, results have shown that these ANNs can be sensitive to individual variation, making generalization outside the training set not straightforward, particularly with amputees. This difficulty may lead to the need to retrain the ANNs with every new user, which may not be possible on amputees as current approaches require specific environments and full arm motion [7]. Furthermore, ANNs extract the common synergies in the training set to create averaged synergies, while optimal synergies for each user exist due to individual variation [9]. In the case of amputees, the optimal use and motion of the prosthesis may not directly reflect the optimal use and motion of the human arm, making the generalization from able-bodied training subjects to prosthetic users more difficult. Furthermore, individuals may experience time varying optimal synergies due to external factors such as fatigue and adaptation through learning.

The need to continuously adjust the setting of a given synergy for an optimal performance leads to the consideration of on-line optimization strategies. Extremum Seeking (ES) is one potentially applicable on-line or data driven optimization method [10]. By using input-output measurements, ES can extract the gradient of an unknown nonlinear mapping and seek an optimum. This feature is relevant to the application as an explicit model of the optimization processes occurring in human motor learning and their influence on the development of synergies is non-existent, and thus the synergy-task nonlinear mapping is unknown. ES has been applied to many engineering applications, see, for example [11], [10] and reference therein. Any parameter identification problem

Ricardo Garcia-Rosas, Ying Tan, Denny Oetomo, and Chris Manzie are with the School of Electrical, Mechanical and Infrastructure Engineering at The University of Melbourne, VIC 3010, Australia. ricardog@student.unimelb.edu.au; {yingt,doetomo,manziec}@unimelb.edu.au

can be also formulated as an optimization problem. Thus ES can be applicable to such problems [12].

In this paper, a framework for on-line data driven optimization is proposed to identify the optimal synergy setting for an individual performing a specific task, formulated as an optimization problem based on human motor control. This is done through the characterization of the task by a cost function and the parametrization of the synergy. This paper shows that the proposed framework is capable of characterizing and identifying the synergy of a reaching task, with a healthy subject in the loop. The framework is used to drive the motion of an elbow prosthesis through its synergy with the residual shoulder motion, i.e. the human subject as input. A basic parametrization for the synergy is used without loss of generality to the proposed framework. The rest of the paper is organized as follows. Section II presents the system description and problem formulation. Section III the proposed methods for task characterization and synergy identification. Section IV the experimental methodology and human-in-the-loop simulation results. Finally, Section V presents concluding remarks and discussion.

The set of real numbers is denoted as $\mathbb{R}$, the set of positive real numbers is denoted as $\mathbb{R}_+$.

## II. System Description

### A. Model for Human-prosthetic arm

In the case of upper limb amputation, an amputee is left with the residual limb which is capable of motion. For instance, in transhumeral amputations (below one's shoulder) [13], the residual limb is composed of the shoulder joints and residual parts of the humerus, biceps and triceps. In this work, the residual limb ($r$) motion is represented by the joint angles $\mathbf{q}_r \in \mathbb{R}^R$, which are given by

$$\mathbf{q}_r = \begin{bmatrix} q_{abd} & q_{fle} & q_{rot} \end{bmatrix}^T, \tag{1}$$

where $R = 3$ is the residual limb's DOF. $q_{abd} \in \mathbb{R}$ represents shoulder abduction/adduction, $q_{fle} \in \mathbb{R}$ shoulder flexion/extension, and $q_{rot} \in \mathbb{R}$ humeral rotation.

The prosthetic device ($p$) motion is represented by the joint angles $\mathbf{q}_p \in \mathbb{R}^P$. In the transhumeral case [13], it is composed of the elbow joint $q_{elb} \in \mathbb{R}$, forearm and hand, where only the elbow is considered in this work. The joints for the whole arm can be represented by the following vector:

$$\mathbf{q} = \begin{bmatrix} \mathbf{q}_r & \mathbf{q}_p \end{bmatrix}^T = \begin{bmatrix} q_{abd} & q_{fle} & q_{rot} & q_{elb} \end{bmatrix}^T, \tag{2}$$

where $\mathbf{q} \in \mathbb{R}^{R+P}$. A representation of this system for the planar case is presented in Figure 1.

The dynamics of the residual limb can be described by the generalized equation of motion of a manipulator as

$$\mathbf{M}_r(\mathbf{q}_r)\ddot{\mathbf{q}}_r + \mathbf{C}_r(\mathbf{q}_r, \dot{\mathbf{q}}_r)\dot{\mathbf{q}}_r + \mathbf{G}_r(\mathbf{q}_r) + \mathbf{Z}_r(\mathbf{q}, \dot{\mathbf{q}}) = \boldsymbol{\tau}_r, \tag{3}$$

where $\mathbf{M}_r \in \mathbb{R}_+^{R\times R}$ is the generalized inertia matrix, which is positive definite and symmetric. The matrix $\mathbf{C}_r \in \mathbb{R}^{R\times R}$ is the Coriolis and centrifugal matrix. The gravity matrix $\mathbf{G}_r$ is in $\mathbb{R}^R$. The matrix $\mathbf{Z}_r \in \mathbb{R}^R$ represents interconnections between the residual limb and prosthesis [14]. The torque vector $\boldsymbol{\tau}_r \in \mathbb{R}^R$ represents muscle torques.

Prosthesis dynamics can be described by the equation:

$$\mathbf{M}_p(\mathbf{q}_p)\ddot{\mathbf{q}}_p + \mathbf{C}_p(\mathbf{q}_p, \dot{\mathbf{q}}_p)\dot{\mathbf{q}}_p + \mathbf{G}_p(\mathbf{q}_p) + \mathbf{Z}_p(\mathbf{q}, \dot{\mathbf{q}}) = \boldsymbol{\tau}_p, \tag{4}$$

where $\mathbf{M}_p \in \mathbb{R}_+^{P\times P}$, $\mathbf{C}_p \in \mathbb{R}^{P\times P}$, $\mathbf{G}_p \in \mathbb{R}^P$, $\mathbf{Z}_p \in \mathbb{R}^P$ represent the respective matrices as in (3), and $\boldsymbol{\tau}_p \in \mathbb{R}^P$ the torque vector representing actuator torque. It is important to note that the matrices in (3), (4) satisfy desirable properties, such as uniform boundedness, as pointed out in [14], [15].

The position of the hand is represented as

$$\mathbf{p} = \begin{bmatrix} p_x & p_y & p_z \end{bmatrix}^T = \mathbf{h}(\mathbf{q}), \tag{5}$$

where the nonlinear mapping $\mathbf{h} : \mathbb{R}^{R+P} \to \mathbb{R}^3$ represents forward kinematics. Hand velocity is represented by:

$$\dot{\mathbf{p}} = \begin{bmatrix} \dot{p}_x & \dot{p}_y & \dot{p}_z \end{bmatrix}^T = \mathbf{J}(\mathbf{q})\dot{\mathbf{q}}, \tag{6}$$

where $\mathbf{J}(\mathbf{q}) \in \mathbb{R}^{3\times(R+P)}$ is the arm Jacobian.

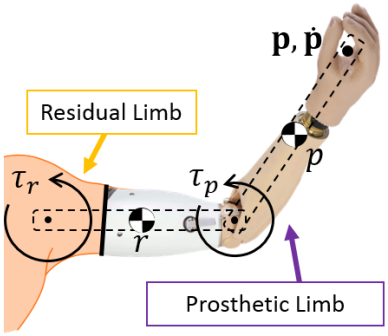


Fig. 1. Human-prosthetic arm diagram.

### B. Human motor control model

Human motor control of the upper limb has properties that allow for the hand to track a reference trajectory in space. That is, for a given hand position, it can track it in steady-state even with unstable interaction forces [16], making it robust to bounded disturbances [17], [18].

Based on [19], a model of human motor control for the residual limb is presented as a summation of three terms:

$$\boldsymbol{\tau}_r = \boldsymbol{\tau}_{idm} + \boldsymbol{\tau}_{fb} + \Delta\boldsymbol{\tau} \tag{7}$$

$$\boldsymbol{\tau}_{idm} = \hat{\mathbf{M}}_r(\bar{\mathbf{q}}_r)\ddot{\bar{\mathbf{q}}}_r + \hat{\mathbf{C}}_r(\bar{\mathbf{q}}_r, \dot{\bar{\mathbf{q}}}_r)\dot{\bar{\mathbf{q}}}_r + \hat{\mathbf{G}}_r(\bar{\mathbf{q}}_r) + \hat{\mathbf{Z}}_r(\bar{\mathbf{q}}, \dot{\bar{\mathbf{q}}}, \ddot{\bar{\mathbf{q}}}) \tag{8}$$

$$\boldsymbol{\tau}_{fb} = -\mathbf{K}_{r,p}(\tilde{\mathbf{q}}_r + r_{sd}\dot{\tilde{\mathbf{q}}}_r). \tag{9}$$

$\tilde{\mathbf{q}}_r = \mathbf{q}_r - \bar{\mathbf{q}}_r$, $\dot{\tilde{\mathbf{q}}}_r = \dot{\mathbf{q}}_r - \dot{\bar{\mathbf{q}}}_r$. $\boldsymbol{\tau}_r$ is the total joint torques given by a feed-forward term $\boldsymbol{\tau}_{idm}$, a feedback term $\boldsymbol{\tau}_{fb}$, and a perturbation term $\Delta\boldsymbol{\tau}$. $\boldsymbol{\tau}_{idm} \in \mathbb{R}^R$ is given by the brain's learned inverse dynamic model of the arm, which includes the learned disturbances related to the prosthetic device. While matrices $\hat{\mathbf{M}}_r$, $\hat{\mathbf{C}}_r$, $\hat{\mathbf{G}}_r$, and $\hat{\mathbf{Z}}_r$ represent the learned dynamics. $\boldsymbol{\tau}_{fb} \in \mathbb{R}^R$ represents muscle stiffness and reflex feedback, and $\Delta\boldsymbol{\tau}$ motor performance variability. $r_{sd} > 0$ is the joint's stiffness-to-damping ratio, and $\mathbf{K}_{r,p}$ is the positive definite joint stiffness matrix given by reciprocal muscle activation and voluntary co-activation [19]. Performance variability is assumed to be bounded by

$$\|\Delta\boldsymbol{\tau}\| < c_v. \tag{10}$$

First, it is assumed that after learning, humans are able to estimate the matrices in (8) well enough. When the inverse dynamic model of the residual limb with attached prosthesis has been learned by the CNS, it can be stated that $\hat{\mathbf{M}}_r = \mathbf{M}_r$, $\hat{\mathbf{C}}_r = \mathbf{C}_r$, $\hat{\mathbf{G}}_r = \mathbf{G}_r$, and $\hat{\mathbf{Z}}_r = \mathbf{Z}_r$; such that the closed

loop dynamics of the residual limb, from equations (3), (7), can be simplified to

$$\ddot{\tilde{\mathbf{q}}}_r = -\mathbf{K}_{r,p}(\tilde{\mathbf{q}}_r + r_{sd}\dot{\tilde{\mathbf{q}}}_r) + \Delta\boldsymbol{\tau}. \tag{11}$$

This can be ensured by providing the user with sufficient training time with the prosthesis, as it has been shown that the CNS can learn and compensate for disturbances [19]. Furthermore, it is clear that, after learning, the dynamics of the residual limb are dominated by the feedback term $\boldsymbol{\tau}_{fb}$. This follows experimental observations with regards to the behavior of the human arm [16].

### C. Prosthesis control

Control of the joints in the prosthesis is usually given by a feedback controller, such as a PD controller with gravity compensation [15].

$$\boldsymbol{\tau}_p = -\mathbf{K}_{p,p}\tilde{\mathbf{q}}_p - \mathbf{K}_{p,d}\dot{\mathbf{q}}_p + \hat{\mathbf{G}}_p(\mathbf{q}_p), \tag{12}$$

where $\mathbf{K}_{p,p}, \mathbf{K}_{p,d}$ are diagonal positive definite stabilizing gains, $\tilde{\mathbf{q}}_p = \mathbf{q}_p - \bar{\mathbf{q}}_p$, and $\bar{\mathbf{q}}_p \in \mathbb{R}^P$ is the desired elbow joint angle. Current prosthetic devices use the signals from an EMG interface to provide the desired joint angle reference; however, for the kinematic synergies approach, the desired angle reference is provided by the kinematic shoulder-elbow synergy. When the gravity compensation term is completely learned, $\hat{\mathbf{G}}_p = \mathbf{G}_p$. Moreover, if the feedback gains $\mathbf{K}_{p,p}$ and $\mathbf{K}_{p,d}$ are sufficiently large such that there exist positive definite diagonal matrices $\Gamma_1$ and $\Gamma_2$, the prosthesis closed loop dynamics, from equations (4), (12), is simplified to

$$\ddot{\tilde{\mathbf{q}}}_p = -\Gamma_1\tilde{\mathbf{q}}_p - \Gamma_2\dot{\mathbf{q}}_p. \tag{13}$$

### D. Kinematic synergies model

Kinematic synergies, in the context of prosthetics, characterize the motion of the prosthetic limb $\dot{\mathbf{q}}_p$ by that of the residual limb $\dot{\mathbf{q}}_r$. This, in general, can be represented by a function parameterized by a family of unknown parameters. These parameters determine a specific kinematic synergy. A general form of kinematic synergies is:

$$\dot{\tilde{\mathbf{q}}}_p = \boldsymbol{\varphi}(\dot{\mathbf{q}}_r, \boldsymbol{\theta}), \tag{14}$$

where $\boldsymbol{\theta} \in \Theta$ are the parameters that determine a specific synergy, $\Theta$ is a compact set in $\mathbb{R}^S$, $S$ the number of synergy parameters, and $\boldsymbol{\varphi} : \mathbb{R}^R \times \Theta \to \mathbb{R}^P$ is known continuously differentiable general synergy function. A shoulder-elbow linear synergy can be parameterized as follows:

$$\dot{\tilde{q}}_{elb} = \varphi(\dot{\mathbf{q}}_r, \boldsymbol{\theta}) = \theta_a\dot{q}_{abd} + \theta_f\dot{q}_{fle} + \theta_r\dot{q}_{rot}. \tag{15}$$

The parameters for a given synergy parameterization are then dependent on the characteristics of the task, desired motion, and the residual limb trajectory. While similarities exist in the motion and synergies of individuals, variations exist as these are affected by a wide range of factors such as preference [9]. Hence, finding a general model that can fit each individual is difficult, even though a large number of data can be collected. Furthermore, synergies in amputees are affected due to the limitations of the device and residual limb compensatory movements that arise from these limitations [20]. Thus a data driven on-line optimization method to iteratively seek the optimal parameter set for a given parameterization, a given task, and an individual subject is proposed in this work.

### E. Problem formulation

The proposed synergistic human-prosthesis arm dynamic system is presented as block diagram in Figure 2. The dynamic system can be represented in state space form as composed by three subsystems, the residual limb dynamics represented by $\Sigma_1$, the synergy dynamics by $\Sigma_2$, and the prosthesis dynamics by $\Sigma_3$.

Consider the residual limb state signals $\boldsymbol{\xi}_1 = \tilde{\mathbf{q}}_r$ and $\boldsymbol{\xi}_2 = \dot{\tilde{\mathbf{q}}}_r$, such that the subsystem representing residual limb closed loop dynamics, from equation (11), $\Sigma_1$, is given by

$$\Sigma_1 \left\{ \begin{bmatrix} \dot{\boldsymbol{\xi}}_1 \\ \dot{\boldsymbol{\xi}}_2 \end{bmatrix} = \begin{bmatrix} \boldsymbol{\xi}_2 \\ -\mathbf{K}_{r,p}(\boldsymbol{\xi}_1 + r_{sd}\boldsymbol{\xi}_2) + \Delta\boldsymbol{\tau} \end{bmatrix}. \right. \tag{16}$$

Due to the boundedness of human variability (10), the trajectories of the system $\Sigma_1$ are globally uniformly bounded.

Let the synergy state be $\boldsymbol{\zeta} = \bar{\mathbf{q}}_p$ such that the subsystem representing synergy dynamics, $\Sigma_2$, is given by

$$\Sigma_2 : \dot{\boldsymbol{\zeta}} = \boldsymbol{\varphi}(\boldsymbol{\xi}_2, \boldsymbol{\theta}), \tag{17}$$

where $\boldsymbol{\theta}$ is the unknown parameter to learn. This system $\Sigma_2$ depends on the state $\boldsymbol{\xi}_2$. From the physical meaning of this system, it is natural to assume that the reference $\boldsymbol{\zeta}$ is uniformly bounded for any $\boldsymbol{\theta} \in \Theta$ and any $\boldsymbol{\xi}_2$ from a predefined compact set. Moreover, the rate of change of the reference provided to the prosthesis controller, $\dot{\boldsymbol{\zeta}}$, is sufficiently slow as it depends on the residual limb. In this work, it is assumed that the set for the unknown parameter is defined as $\Theta = \{\boldsymbol{\theta} \mid \underline{\boldsymbol{\theta}} \leq \boldsymbol{\theta} \leq \bar{\boldsymbol{\theta}}\}$, where $\underline{\boldsymbol{\theta}}$ and $\bar{\boldsymbol{\theta}}$ are the lower and upper bounds of $\boldsymbol{\theta}$ respectively. Thus enforcing that the reference provided to the prosthesis controller remains within the set of interest.

Finally, let the prosthesis state be $\boldsymbol{\eta}_1(\boldsymbol{\zeta}) = \tilde{\mathbf{q}}_p(\boldsymbol{\zeta})$ and $\boldsymbol{\eta}_2 = \dot{\mathbf{q}}_p$, such that the subsystem representing prosthesis closed loop dynamics, from equation (13), $\Sigma_3$, is approximated by

$$\Sigma_3 : \left\{ \begin{bmatrix} \dot{\boldsymbol{\eta}}_1 \\ \dot{\boldsymbol{\eta}}_2 \end{bmatrix} = \begin{bmatrix} \boldsymbol{\eta}_2 \\ -\Gamma_1\boldsymbol{\eta}_1 - \Gamma_2\boldsymbol{\eta}_2 \end{bmatrix}. \right. \tag{18}$$

Moreover, it is assumed that the stability properties of $\Sigma_3$ are uniform with respect to any $\boldsymbol{\zeta}$ that is within a compact set of interest.

It is noted that the focus of this work is not stability of the overall system as boundedness of the three systems has already been achieved, which is also observed in experiments. The focus is finding an optimal set of parameters for a given parameterization for each individual repeating the same task many times. Even though the proposed parameterization might not be the best for this setting, with the proposed on-line parameter identification technique, the best parameter set can still be identified using the input-output measurements under the given parameterization; provided that the optimal parameter set is iteration invariant or slowly changing over iterations. In order to do on-line parameter identification, an appropriate cost function is needed. Next, the problem is formulated as an optimization problem.

When a point-to-point tracking task is considered, the cost is related to tracking performance. That is, finding an optimal set of parameters if a human subject repeats the task many times. More precisely, arm motion with hand target $\bar{\mathbf{p}}_f$, initial conditions $\boldsymbol{\xi}_1(T_o)$, $\boldsymbol{\eta}_1(T_o)$, and residual limb

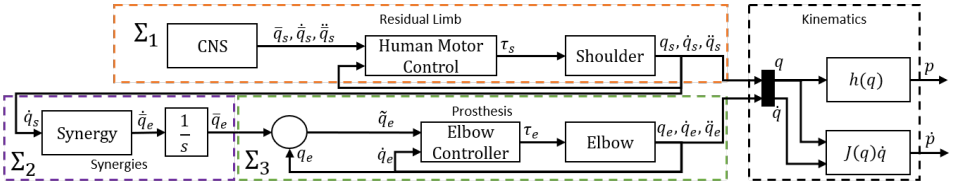


Fig. 2. Synergistic human-prosthesis arm block diagram.

trajectory $\boldsymbol{\xi}_1(t) \forall t \in [T_o, T_f]$ is considered. The objective is to determine the optimal synergy parameters $\boldsymbol{\theta}^*$ over iterations (or by repeating the same task over the iteration domain) such that the hand reaches a small neighbourhood of the desired target by the end of motion, i.e. $\mathbf{p}^{(i)}(T_f) \to \bar{\mathbf{p}}_f$ as the iteration number $i$ goes to infinity.

## III. Task Characterization and On-line Kinematic Synergy Identification

In order to simplify the presentation, a reaching task is considered. The similar idea can be applied to more complex tasks with appropriate modifications. Furthermore, most Activities of Daily Living (ADLs) require some sort of reaching motions. Many others, such as eating, consist of repetitive reaching motions.

### A. Reaching task characterization

A point-to-point reaching task is described by the desired hand start and end positions $\bar{\mathbf{p}}_o \in \mathbb{R}^3$, $\bar{\mathbf{p}}_f \in \mathbb{R}^3$ respectively. Usually, the time taken to reach the end position will be ignored. Other than tracking accuracy, the quality of the motion, typically represented by jerk $\dddot{\mathbf{p}}(t)$, is also considered, where $t \in [t_o, t_f]$, $t_f \leq t_{f,max}$ for a given $t_{f,max}$.

The number of iterations is represented by the superscript $i$. E.g. the hand trajectory at the $i^{th}$ iteration is denoted as $\mathbf{p}^i(t)$. It is assumed that $\bar{\mathbf{p}}_o$ and $\bar{\mathbf{p}}_f$ can be determined through an initialization or teaching phase where the user manually moves the prosthesis to the desired start and end positions, such as is the case with training environments.

In general, this set of motion characteristics can be represented as a cost function that linearly combines the motion objectives [21]. Let the task cost function be given by

$$J(\boldsymbol{\theta}) = \sum_{j=1}^{n} \alpha_j \psi_j, \tag{19}$$

where $n > 0$ is the number of motion characteristics considered, and $\alpha_j > 0$ the weight given to each characteristic. The nonlinear mapping $\psi_j : \mathbb{R}^{M_j} \to \mathbb{R}_+$ represents a desired motion characteristic, where $M_j$ is the dimension of the arguments of $\psi_j$. It is assumed that each motion objective is related to the task and thus the synergy, i.e., $\psi_j = \psi_j(\boldsymbol{\theta})$, though an explicit model of this relationship is unavailable. Moreover, it is also assumed that the cost function is measurable at each iteration. It is assumed that the format of this cost function is iteration-invariant, or very slow changing over iteration domain.

Typical motion characteristics are target error (20) and hand jerk (21) [21]. Here, $\psi_1$ is the tracking error and $\psi_2$ is the jerk of hand movements.

$$\psi_1 = \|\mathbf{p}^i(T_f^i) - \bar{\mathbf{p}}_f\|^2 \tag{20}$$

$$\psi_2 = \int_{T_o}^{T_f^i} \|\dddot{\mathbf{p}}^i(t)\|^2 dt, \tag{21}$$

$T_o$ is the motion start time, which is iteration invariant, and $T_f^i > 0$ is the iteration varying motion end time satisfying $t_o \leq T_o \leq T_f^i \leq t_{f,max}$.

From equation (5) and the systems $\Sigma_1$, $\Sigma_2$, and $\Sigma_3$, it is clear that hand trajectory $\mathbf{p}(t)$ is a function of the residual limb trajectory $\boldsymbol{\xi}_1(t)$ and synergy parameterization $\boldsymbol{\theta}$. It has been shown that after learning, human motor behavior converges to a region around an optimal motion and motion completion time [22], such that given an optimal residual limb trajectory $\boldsymbol{\xi}_1^*(t)$ and end time $T_f^*$ the following inequalities hold

$$\|\boldsymbol{\xi}_1^i(t) - \boldsymbol{\xi}_1^*(t)\| \leq \Delta_q \tag{22}$$

$$\|T_f^i - T_f^*\| \leq \Delta_t, \tag{23}$$

where $\Delta_q, \Delta_t > 0$. Then, a function composed of $\psi_1$ and $\psi_2$ has a unique extremum when $\boldsymbol{\xi}_1(t) = \boldsymbol{\xi}_1^*(t)$ and $\boldsymbol{\theta} = \boldsymbol{\theta}^*$.

**Remark 1.** *The optimal motion $\boldsymbol{\xi}_1^*(t)$ and time $T_f^*$ vary among individuals, and so do $\Delta_q$ and $\Delta_t$. Particularly, $\Delta_q$ is a function of the motion performance variation $\Delta\boldsymbol{\tau}$ of each individual.* ○

### B. On-line kinematic synergy identification

It is clear from the physical properties of systems $\Sigma_1$, $\Sigma_2$, and $\Sigma_3$ that the system is stable by ensuring $\boldsymbol{\theta}$ remains in the domain of interest with the projection method. By allowing the human sufficient training time to learn the task and its dynamics, equations (22) and (23) hold, and thus the cost function $J(\boldsymbol{\theta})$ has a unique extremum when $\boldsymbol{\theta} = \boldsymbol{\theta}^*$. Therefore, the system satisfies Assumptions 1-3 in [23].

Given the iterative nature of the problem, discrete-time ES [24] is suitable to the problem. Even though the task is iterative in task space, it is not necessarily finished within the same time interval in every iteration. However, in controlled environments, e.g. training, a fixed completion time can be set to every iteration such that $T_f^i = t_{f,max}$. Thus the conditions for discrete-time ES in [24], [25] are satisfied.

An important aspect of the problem is the performance variation introduced by having a human-in-the-loop. This variation is reflected in the gradient of the cost function as a bounded non-vanishing perturbation. As has been discussed in [26], when this perturbation is sufficiently small (in this work $\Delta_q$) stability and semi-global asymptotic convergence of the system is not affected. This can be satisfied by allowing sufficient training time for the human to learn the task and dynamics of the system.

Even though the task cost function is estimated by the selected cost function in (19), the explicit relationship between $J$ and $\theta$ is unknown. Thus a discrete-time ES algorithm is used to estimate the gradient $\frac{\partial J}{\partial \theta}$ using only input-output measurements. By tuning parameters appropriately,

the output of ES will converge to a small neighborhood of the optimal value. As the gradient method is used, local or regional convergence can be achieved. The diagram of the proposed on-line parameter estimation method is presented in Figure 3. Subscript $k = \{1, 2, \ldots, S\}$ represents each parameter to be estimated, and thus one ES loop is used for each parameter.

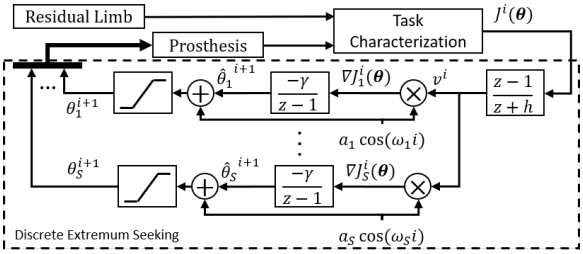

Fig. 3. On-line synergy identification.

From this figure, the updating laws, for each ES loop $k$, can be presented as follows

$$v^i = -hv^{i-1} + J^i(\boldsymbol{\theta}) - J^{i-1}(\boldsymbol{\theta}) \quad (24)$$

$$\hat{\theta}_k^{i+1} = \hat{\theta}_k^i - \gamma a_k \cos(\omega_k i) v^i \quad (25)$$

$$\theta_k^{i+1} = \begin{cases} \underline{\theta}_k, & \hat{\theta}_k^{i+1} < \underline{\theta}_k \\ \bar{\theta}_k, & \hat{\theta}_k^{i+1} > \bar{\theta}_k \\ \hat{\theta}_k^{i+1} + a_k \cos(\omega_k i) & \text{else} \end{cases}. \quad (26)$$

$\omega_k$ represents the dither frequency for each ES loop, satisfying the condition that they are not equal to each other, or their linear combinations [11]. $a_k \in \mathbb{R}$ is the dither amplitude. $0 < h < 1$ is the high pass filter cutoff frequency, which should be smaller than the smallest dither frequency $\omega_k$. $\gamma > 0$ is a parameter related to the convergence speed of the algorithm. Equation (26) denotes the update law with projection on $\boldsymbol{\theta}$ to ensure the condition $\boldsymbol{\theta} \in \Theta$. The structure of ES in Figure 2 is similar to [24], [25], with the extra projection block added.

**Remark 2.** *The dither frequencies $\omega_k$ are selected such that the following inequalities are satisfied*

$$\omega_k \neq \omega_p, \quad p \neq k, \quad k, p = \{1, \ldots, S\} \quad (27)$$

$$\omega_k \neq \omega_p + \omega_r, \quad \forall k, p, r = \{1, \ldots, S\}, \quad (28)$$

*in order to ensure sufficient persistency of excitation.* ○

## IV. Human-in-the loop experimental results

The experiment was designed to emulate a transhumeral amputee wearing an elbow prosthesis, as shown in Figure 4, by only considering motion of the upper arm of able-bodied subjects. In order to check the feasibility of the proposed framework, a simple human-in-the-loop experiment was performed. The experiment was performed with two able-bodied subjects, one male (28) and one female (25). Measurements of the upper arm motion were obtained using Thalmic Labs' Myoband IMU [27], which provided shoulder joint position $\mathbf{q}_r$ and velocity $\dot{\mathbf{q}}_r$. The task consisted of a forward reaching task to be repeated 75 times.

A real-time human-in-the-loop simulation was done in MATLAB/Simulink 2017a on an Intel Corei7-6600 at 2.60GHz, 16.0GB of RAM. The simulation sample time was $\Delta t = 0.02s$ with user interface (UI) refresh rate of $0.1s$. Upper arm motion was measured at every sample. The UI

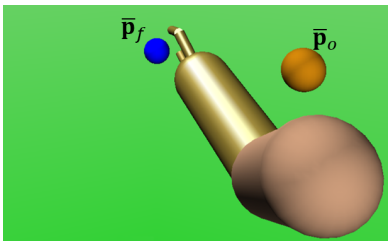

Fig. 4. Experiment GUI.

showed a first person view of the target and arm, as shown in Figure 4, where the orange ball represents the starting point $\bar{\mathbf{p}}_o$ and the blue ball the target $\bar{\mathbf{p}}_f$.

Subjects were allowed training time with the task and environment in order to satisfy the conditions established in Section III-B. The maximum time allowed for completion of motion was set to five seconds $t_{f,max} = 5$. A linear synergy parameterization, as presented in equation (15), was chosen. Synergy parameters were initialized at zero $\boldsymbol{\theta}^1 = 0$. The cost function consisted of tracking error $\psi_1$ and hand jerk $\psi_2$, equations (20) and (21) respectively. The weights used in the cost function were $\alpha_1 = 1$, $\alpha_2 = 0.1$. The following tuning parameters for ES algorithm were used $h = 0.001$, $\gamma = 30$, $w_1 = 0.8\pi$, $w_2 = \pi$, $w_3 = 0.6\pi$, $a_1 = a_2 = a_3 = 0.1$. $\boldsymbol{\theta}$ projection was set to $\bar{\boldsymbol{\theta}} = 1$ and $\underline{\boldsymbol{\theta}} = -2$.

Results for Subject 1 are presented with solid lines, while Subject 2 with dotted lines. Figure 5 shows an example of the shoulder trajectory followed in one iteration of the task, which is obviously bounded. The iteration chosen for comparison showed similar performance for both subjects. From this it is possible to observe the difference in strategy followed by each subject. This is reflected in the elbow trajectory arising from the synergy, as shown in Figure 6.

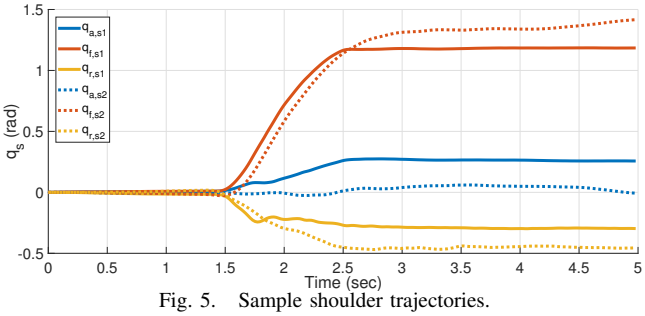

Fig. 5. Sample shoulder trajectories.

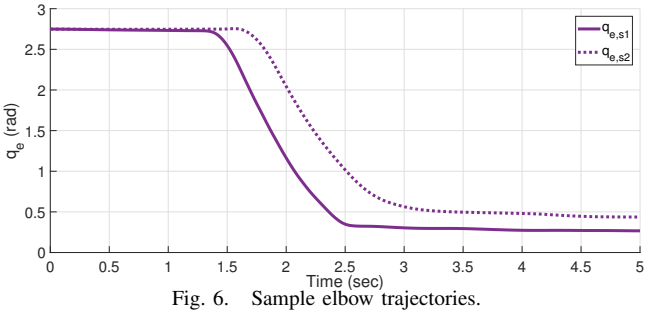

Fig. 6. Sample elbow trajectories.

Figure 7 shows the evolution of the synergy parameters throughout iterations while Figure 8 the value of the cost function. As expected, the difference in motion strategy followed by each subject is reflected in the optimal synergy parameters. This suggests that learning from individual data is thus needed to address variability coming from human

subjects. Any model from averaged behaviors will have problems. It is also noted that similarities can still be observed. An important observation arises in the results for Subject 2 in Figure 8 between iterations 20 and 40, where performance variation was significantly higher than in other iterations. This in turn can be observed in the convergence of the ES algorithm, as is shown in Figure 7 within the same iterations. This behavior is expected as human performance variation is reflected in the cost function as a bounded perturbation, and in turn affects the boundary of convergence of the ES algorithm. Subjects were given sufficient training time to mitigate the transient behavior introduced by human motor learning and reduce performance variability. However, in a practical application, human learning will need to be considered if the system is to adapt to a range of individuals. This motivates future research directions in developing methods for handling short term human variation and long term learning behavior in human-in-the-loop ES systems.

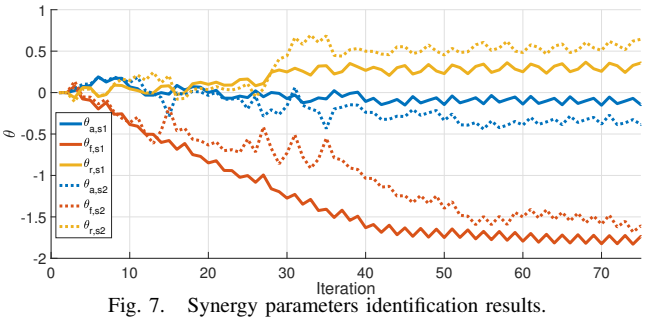

Fig. 7. Synergy parameters identification results.

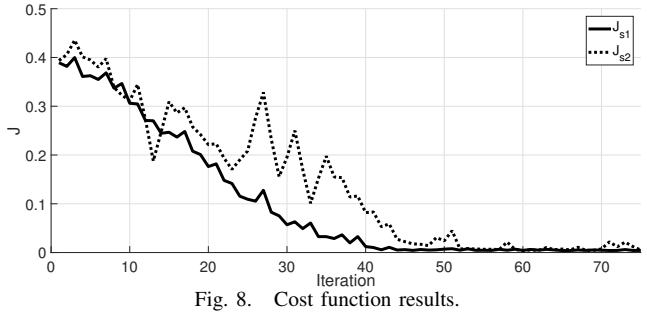

Fig. 8. Cost function results.

## V. Conclusion

A framework for on-line data driven optimization was proposed to identify the optimal synergy for an individual performing a specific task during repeated use. An example of task characterization and synergy parameterization was demonstrated with a basic forward reaching task and linear shoulder-elbow synergy. Human-in-the-loop simulation results were presented, showing the feasibility of data driven optimization for on-line synergy identification. Future work will explore methods to handle human variability outside controlled training environments and during the learning phase. Moreover, the analysis of different task characterizations, synergy parameterizations and the long term performance of the algorithm warrants investigation.

## References


[1] T. A. Kuiken, "Targeted Muscle Reinnervation for Real-time Myoelectric Control of Multifunction Artificial Arms," *J. Am. Med. Assoc.*, vol. 301, no. 6, p. 619, 2009.

[2] E. Biddiss and T. Chau, "Upper-limb prosthetics: critical factors in device abandonment.," *Am. J. Phys. Med. Rehabil.*, vol. 86, no. 12, pp. 977–987, 2007.

[3] J. F. Soechting and F. Lacquaniti, "An assessment of the existence of muscle synergies during load perturbations and intentional movements of the human arm," *Exp. Brain Res.*, vol. 74, no. 3, pp. 535–548, 1989.

[4] M. Tagliabue, A. L. Ciancio, T. Brochier, S. Eskiizmirliler, and M. A. Maier, "Differences between kinematic synergies and muscle synergies during two-digit grasping.," *Front. Hum. Neurosci.*, vol. 9, p. 165, 2015.

[5] R. R. Kaliki, R. Davoodi, and G. E. Loeb, "Evaluation of a noninvasive command scheme for upper-limb prostheses in a virtual reality reach and grasp task," *IEEE Trans. Biomed. Eng.*, vol. 60, no. 3, pp. 792–802, 2013.

[6] W. D. I. G. Dasanayake, R. A. R. C. Gopura, V. P. C. Dassanayake, and G. K. I. Mann, "Estimation of prosthetic arm motions using stump arm kinematics," in *Int. Conf. Inf. Autom. Sustain.*, pp. 1–6, 2014.

[7] M. Merad, E. de Montalivet, A. Roby-Brami, and N. Jarrasse, "Intuitive prosthetic control using upper limb inter-joint coordinations and IMU-based shoulder angles measurement: A pilot study," in *IEEE/RSJ Int. Conf. Intell. Robot. Syst.*, pp. 5677–5682, 2016.

[8] A. Akhtar, N. Aghasadeghi, L. Hargrove, and T. Bretl, "Estimation of distal arm joint angles from EMG and shoulder orientation for transhumeral prostheses," *J. Electromyogr. Kinesiol.*, vol. 35, pp. 86–94, 2017.

[9] L. Tang, F. Li, S. Cao, X. Zhang, and X. Chen, "Muscle synergy analysis for similar upper limb motion tasks," in *Conf. IEEE Eng. Med. Biol. Soc.*, pp. 3590–3593, 2014.

[10] Y. Tan, W. Moase, C. Manzie, D. Nesic, and I. Mareels, "Extremum seeking from 1922 to 2010," *Chinese Control Conf.*, pp. 14–26, 2010.

[11] K. B. Ariyur and M. Krstić, *Real-Time Optimization by Extremum-Seeking Control*. Wiley, 2003.

[12] A. Scheinker and S. Gessner, "Extremum seeking for parameter identification, implementation for electron beam property prediction," in *IEEE Conf. Decis. Control*, vol. 2015-Febru, pp. 2673–2678, 2014.

[13] A. Fougner, O. Stavdahl, P. J. Kyberd, Y. G. Losier, and P. A. Parker, "Control of Upper Limb Prostheses: Terminology and Proportional Myoelectric Control - A Review," *IEEE Trans. Neural Syst. Rehabil. Eng.*, vol. 20, no. 5, pp. 663–677, 2012.

[14] Y. Tang, M. Tomizuka, G. Guerrero, and G. Montemayor, "Decentralized robust control of mechanical systems," *IEEE Trans. Automat. Contr.*, vol. 45, no. 4, pp. 771–776, 2000.

[15] R. Kelly, "PD Control with Desired Gravity Compensation of Robotic Manipulators: A Review," *Int. J. Rob. Res.*, vol. 16, no. 5, pp. 660–672, 1997.

[16] J. Won and N. Hogan, "Stability properties of human reaching movements.," *Exp. Brain Res.*, vol. 107, no. 1, pp. 125–136, 1995.

[17] E. Burdet, R. Osu, D. W. Franklin, T. E. Milner, and M. Kawato, "The central nervous system stabilizes unstable dynamics by learning optimal impedance," *Nature*, vol. 414, no. 6862, pp. 446–449, 2001.

[18] S.-H. Zhou, D. Oetomo, Y. Tan, E. Burdet, and I. Mareels, "Modeling individual human motor behavior through model reference iterative learning control.," *IEEE Trans. Biomed. Eng.*, vol. 59, no. 7, pp. 1892–901, 2012.

[19] E. Burdet, K. P. Tee, I. Mareels, T. E. Milner, C. M. Chew, D. W. Franklin, R. Osu, and M. Kawato, "Stability and motor adaptation in human arm movements," *Biol. Cybern.*, vol. 94, no. 1, pp. 20–32, 2006.

[20] S. Micera, J. Carpaneto, F. Posteraro, L. Cenciotti, M. Popovic, and P. Dario, "Characterization of upper arm synergies during reaching tasks in able-bodied and hemiparetic subjects," *Clin. Biomech.*, vol. 20, no. 9, pp. 939–946, 2005.

[21] D. A. Kistemaker, J. D. Wong, and P. L. Gribble, "The cost of moving optimally: kinematic path selection," *J. Neurophysiol.*, vol. 112, no. 8, pp. 1815–1824, 2014.

[22] G. Sebastian, J. Fong, V. Crocher, Y. Tan, D. Oetomo, and I. Mareels, "Quantifying task similarity for skill generalisation in the context of human motor control," in *Int. Conf. Control. Autom. Robot. Vis.*, 2016.

[23] Y. Tan, D. Nešić, and I. Mareels, "On non-local stability properties of extremum seeking control," *Automatica*, vol. 42, no. 6, pp. 889–903, 2006.

[24] J.-Y. Choi, M. Krstic, K. Ariyur, and J. Lee, "Extremum seeking control for discrete-time systems," *IEEE Trans. Automat. Contr.*, vol. 47, no. 2, pp. 318–323, 2002.

[25] N. Killingsworth and M. Krstic, "PID tuning using extremum seeking: online, model-free performance optimization," *IEEE Control Syst. Mag.*, vol. 26, no. 1, pp. 70–79, 2006.

[26] S. Z. Khong, D. Nešić, and M. Krstić, "Iterative learning control based on extremum seeking," *Automatica*, vol. 66, pp. 238–245, 2016.

[27] Thalmic Labs, "Myo Band," *https://www.myo.com/*, 2018.